Published in final edited form as:
ACS Chem Biol. 2012 June 15; 7(6): 1059–1066. doi:10.1021/cb3000265.

Tyrosine crosslinking reveals interfacial dynamics in adeno-associated viral capsids during infection

Eric D. Horowitz[1], **M.G. Finn**[4], and **Aravind Asokan**[1,2,3,*]

[1]Gene Therapy Center, The University of North Carolina at Chapel Hill, Chapel Hill, NC

[2]Department of Genetics, The University of North Carolina at Chapel Hill, Chapel Hill, NC

[3]Department of Biochemistry & Biophysics, The University of North Carolina at Chapel Hill, Chapel Hill, NC

[4]Department of Chemistry and The Skaggs Institute of Chemical Biology, The Scripps Research Institute, La Jolla, CA

Abstract

Viral capsid dynamics are often observed during infectious events such as cell surface attachment, entry and genome release. Structural analysis of adeno-associated virus (AAV), a helper-dependent parvovirus, revealed a cluster of surface-exposed tyrosine residues at the icosahedral two-fold symmetry axis. We exploited the latter observation to carry out selective oxidation of Tyr residues, which yielded crosslinked viral protein (VP) subunit dimers, effectively "stitching" together the AAV capsid two-fold interface. Characterization of different Tyr-to-Phe mutants confirmed that the formation of crosslinked VP dimers is mediated by dityrosine adducts and requires the Tyr704 residue, which crosses over from one neighboring VP subunit to the other. When compared to unmodified capsids, Tyr-crosslinked AAV displayed decreased transduction efficiency in cell culture. Surprisingly, further biochemical and quantitative microscopy studies revealed that restraining the two-fold interface hinders externalization of buried VP N-termini, which contain a phospholipase A2 domain and nuclear localization sequences critical for infection. These adverse effects caused by tyrosine oxidation support the notion that interfacial dynamics at the AAV capsid two-fold symmetry axis play a role in externalization of VP N-termini during infection.

Conformational changes in the non-enveloped capsids of adenovirus and rotavirus have been associated with critical events during infection (1, 2, 3, 4). Similarly, rearrangements of viral protein (VP) subunits have been postulated in the case of parvoviruses subsequent to cell entry (5, 6, 7). Adeno-associated viruses are small, helper-dependent parvoviruses packaging a 4.7kb ssDNA genome (8). The single-layered, T=1 icosahedral shell is assembled from three overlapping viral proteins (VPs), VP1, VP2 and VP3, which are generated from overlapping reading frames in the *cap* gene. A total of 60 copies of VP1 (87kDa), VP2 (72kDa) and VP3 (62kDa) (Figure 1A) in a predicted ratio of 1:1:10 form the AAV capsid (9, 10, 11). The overlapping VP3 amino acids, which share the same C-terminal amino acid sequence with VP1/VP2 subunits, contain the molecular determinants for receptor binding, tissue tropism, and antigenicity.

*Corresponding Author: Aravind Asokan CB # 7352, Gene Therapy Center, 5123 Thurston Building The University of North Carolina at Chapel Hill Chapel Hill, NC 27599-7352 Tel. No: 919-843-7621 Fax No: 919-966-0907 aravind@med.unc.edu.

Supporting Information available: This material is available free of charge *via* the Internet at http://pubs.acs.org.

The VP1 subunit contains an extended N-terminal unique domain (VP1u) that displays phospholipase A2 (PLA2) activity. In addition, the extended VP1/VP2 subunits contain a common region that contains a cluster of positively charged motifs comprised of basic amino acid residues, which have been implicated in assembly, intracellular trafficking and nuclear entry of AAV serotype 2 (AAV2) vectors (12, 13, 14). Externalization of the AAV2 VP1u domain, which remains buried within the capsid prior to cellular uptake, is essential for endosomal escape and subsequent nuclear entry (5, 13, 15, 16). However, insights into the structural and cellular mechanisms that trigger this event have remained elusive.

Structural studies of different AAV serotypes have revealed that the characteristic surface features on AAV capsids are formed by variable loop regions located between eight β-strands in each monomer subunit (17, 18, 19, 20, 21). These studies have also established that inter-subunit interactions at the two-fold and five-fold icosahedral symmetry axis are more conserved than those utilized for three-fold interactions. Further, calculations of buried surface areas between AAV capsid subunit monomers at different interfaces show that inter-subunit interactions are least prevalent at the two-fold interface and most extensive at the three-fold symmetry axis (18). In the current report, we have utilized a chemical approach, which involves covalent crosslinking of adjacent tyrosine residues (22), to interrogate AAV capsid dynamics. Owing to the clustering of tyrosine residues at the two-fold interface of AAV2 capsids, this chemical strategy effectively “stitched” capsid protein subunits together, resulting in decreased conformational flexibility. Crosslinked capsids demonstrate attenuated externalization of the VP1u domain and decreased transduction efficiency *in vitro*. The studies described herein corroborate a critical role for conformational changes at the two-fold interface in VP1u domain externalization and efficient transduction of AAV vectors.

RESULTS AND DISCUSSION

Tyrosine cluster at the two-fold interface

Phosphorylation of surface-exposed tyrosine residues in VP subunits has been shown to target AAV capsids for proteasomal degradation (23). In these studies, mutation of surface-exposed tyrosines to phenylalanines reduced ubiquitination of VP subunits and enhanced AAV2 transduction by varying levels. Amongst these residues, Tyr700, Tyr704 and Tyr730 are clustered within a single polypeptide loop at the two-fold symmetry axis. The two-fold interface located between VP dimers is the weakest region on the icosahedral AAV capsid and is comprised of a single polypeptide loop (W694-N705) derived from each neighboring VP subunit (18). A surface rendering of two neighboring VP trimers is shown within the context of the AAV2 capsid (Figure 1B). As seen in Figure 1C, a close up view of the dimer of trimers reveals different surface-exposed tyrosine residues in each neighboring VP subunit (red or blue) with Y700/Y704/Y730 clustering together at the two-fold interface (white border). The Y704 residue extending from each VP monomer into the neighboring subunit is highlighted (white arrows). These structural attributes provided the rationale for exploring tyrosine-specific crosslinking chemistries as a strategy to selectively constrain conformational changes at the two-fold symmetry axis.

Tyrosine crosslinking yields VP dimers

Oxidative tyrosine crosslinking has previously been utilized as a tool to probe the multimeric structure of proteins such as RNase (24) and the bacteriophage Qβ (22). The underlying chemistry involves use of nickel(II) salts to mediate the crosslinking of proteins in the presence of a free radical source. Once oxidized, the Ni(III) ion, stabilized by a short Gly-Gly-His tripeptide, extracts an electron from a solvent accessible tyrosine to give a tyrosyl radical that can be captured by a neighboring phenolic side chain, giving dityrosine

units (24, 25) (Figure 2A). We postulated that this covalent crosslinking of tyrosine residues within the AAV capsid, which are clustered predominantly near the two-fold interface, would selectively restrain potential conformational changes that occur at that interface. Upon crosslinking under optimal reaction conditions (22), we observed inter-subunit VP dimers of different molecular weights (MW) as determined by western blot analysis with the B1 monoclonal antibody (MAb), which recognizes all three VP subunits (Figure 2B). As shown in Figure 2B, premixing the chemical reagents was suboptimal due to the formation of capsid protein precipitates, which were not resolved by electrophoresis. In contrast, the sequential addition of MMPP to Ni/GGH in the presence of AAV2 particles provided optimal reaction conditions for crosslinked VP dimer formation. Although we observed some crosslinking in the absence of oxidant, this effect was completely abolished when a reducing agent (L-Cysteine) was added (data not shown). This might suggest the presence of an adventitious oxidant in the reaction. No inter-capsid crosslinking was observed under these optimal conditions as demonstrated by the absence of capsid aggregates in electron micrographs (Supplementary Figure S1). Further, no significant loss of viral titer was observed due to crosslinking (Supplementary Table S2). In addition to protein bands that correspond to VP1, VP2 and VP3 monomer subunits, higher MW protein bands were identified as VP1–VP3 (146kDa), VP2–VP3 (134kDa), and VP3-VP3 (124kDa) dimers (Figure 2B). Due to the ~10-fold lower levels of VP1/VP2 subunits relative to the VP3 subunit alone, we were only able to observe additional VP1-VP1 (168kDa) and VP1–VP2 (157kDa) dimers when using A1/A69 MAbs, which recognize the VP1/VP2 N-terminal domain (26) (Figure 2C & 2D). The VP2-VP2 dimers (144kDa) were likely indistinguishable from VP1–VP3 dimers (146kDa). Densitometric analysis of VP subunit bands visualized by colloidal blue® staining indicates that dimers containing at least one VP3 subunit constitute the major crosslinked species and that ~50% of VP subunits on the capsid are crosslinked to form dimers (Figure 2E & 2F).

Tyr704 mediates formation of crosslinked VP dimers

In order to determine which residues are involved in the formation of crosslinked VP dimers, we used site-directed mutagenesis to mutate Tyr residues to Phe, which is inert to Ni(II)-mediated chemical modification (22). Based on structural cues described earlier (Figure 1B), we generated Tyr-to-Phe mutations at positions 700, 704, and 730 (VP1 numbering), all of which cluster together at the two-fold interface. As mentioned earlier, these residues were previously modified by Srivastava and others (23). Consistent with these previous reports, AAV2 mutants Y700F, Y704F, and Y730F packaging a chicken β-actin promoter-driven luciferase (CBA-Luc) transgene cassette yielded viral titers comparable to unmodified AAV2 vectors (Supplementary Table S2).

The Tyr-to-Phe mutants were subjected to crosslinking and different VP subunits analyzed using western blot analysis using B1 and A1 MAbs as described earlier. As seen in Figure 3A, each Tyr-to-Phe mutant displayed markedly different crosslinking efficiency in comparison with wild type AAV2 capsids. Notably, the Y700F mutant demonstrated robust crosslinking as indicated by the decreased intensity of protein bands corresponding to VP monomer subunits as well as higher MW VP dimers. In contrast, the Y704F mutation completely abolished crosslinking as evidenced by the lack of higher MW VP dimers. These observations are further corroborated by western blot analysis with the A1 MAb, which detects the VP1u region (Figure 3B). The Y730F mutant is not recognized by the B1 MAb, since Y730 lies within the the B1 epitope, but displayed significant crosslinking efficiency as evidenced by A1 MAb staining shown in Figure 3B. These results corroborate the notion that crosslinked VP dimers are indeed formed due to dityrosine adducts at the two-fold interface. Further, crosslinked AAV2 vectors displayed gene transfer efficiency (luciferase transgene expression levels) approximately 1 log unit lower than their unmodified

counterparts in HEK 293 cells at 24hrs post-transduction (Figure 3C). The mutants Y700F and Y730F show a similar decrease in transduction efficiency (~ 1 log unit) after crosslinking, consistent with western blot analysis. In contrast, gene transfer efficiency of the Y704F mutant only shows a slight decrease (<2-fold) upon crosslinking, confirming the absence of crosslinked VP subunit dimers. These results are further supported by measuring the distances between the 3′ carbon atoms on different tyrosine residues. As seen in Figure 3D, the inter-subunit distances are 10Å, 13Å and 21Å between Y704 and Y730, Y700 and Y704 respectively. These observations suggest that the formation of inter-subunit dityrosine adducts is most likely due to free radical crosslinking of the Tyr704 residue in one VP subunit with either Y700 or Y730 residues in the neighboring subunit (Figure 3D).

Crosslinking blocks VP1u domain externalization

Prior to infection, the AAV2 VP1u domain reported to be buried within the capsid interior and is thus inaccessible to the A1 antibody (5, 6). Externalization of the VP1u domain, which has been shown to possess phospholipase A2 (PLA2) activity and nuclear localization signals, is critical for endosomal escape and nuclear entry of AAV vectors (12, 13, 14). Several reports have demonstrated that the VP1u domain is externalized upon limited heat shock and that conformational changes that lead to this irreversible event are blocked in certain AAV capsid five-fold mutants (5, 6). Externalization of the VP1u domain was determined through immunoblot analysis with the A1 MAb, which detects residues 123–130 in the VP1 N-terminal region along with the A20 MAb, which detects a conformational epitope maintained only in intact AAV2 capsids as an internal standard (26). Both unmodified and crosslinked AAV2 capsids were heated to different temperatures and immunoblots quantitated using densitometric analysis (Figure 4). Loss of A20 recognition, which correlates with disruption of tertiary and quaternary structure of both unmodified and crosslinked AAV2 capsids begins at ~55 °C (Figure 4A). In contrast, externalization of the VP1u domain, as evidenced by a gain in A1 recognition beginning at ~60 °C, is observed only with unmodified AAV2, but not tyrosine-crosslinked capsids (Figure 4B). Overall, these observations support the notion that conformational restraint at the two-fold interface blocks externalization of the VP1u domain.

Confocal microscopy studies have been utilized to determine intracellular trafficking defects of various AAV mutants (12, 13, 14). Using confocal immunofluorescence microscopy, we observed similar intracellular trafficking patterns, characterized by perinuclear accumulation for both unmodified and crosslinked AAV2 vectors at 20hrs post-infection in HeLa cells (Figure 5A & 5D). Immunostaining of the VP1u (amino acids 2–16) domain with an anti-VP1u MAb (14) shows co-localization of exposed VP1u with A20 immunostaining for unmodified AAV2 capsids (Figure 5B & 5C). In contrast, crosslinked capsids show low levels of exposed VP1u domains (Figure 5E & 5F). The mean VP1u fluorescence intensity (red signal) normalized to the mean capsid fluorescence intensity (green signal) per cell were calculated using ImageJ® software. Histograms of normalized fluorescence intensities for unmodified and crosslinked AAV2 capsids are shown in Figure5G and 5H, respectively. Approximately 15% of the cells transduced with unmodified AAV2 capsids are observed at low peak intensity (0.1) and an additional 15% at higher peak intensity (0.4) (Figure 5G). In contrast, nearly twice as many cells (~30%) transduced with crosslinked AAV2 capsids are observed at low peak intensity (0.1) and only 5% with higher peak intensity (0.4) (Figure 5H). The latter results confirm that plasticity of the two-fold interface is essential for exposure of the buried VP1u domain during intracellular trafficking of AAV2 virions. Further, these results provide insight into the putative mechanism underlying decreased transduction efficiency of tyrosine-crosslinked AAV2 virions *in vitro* (Figure 3C).

Mechanisms of VP1 N-terminal domain exposure

The VP1 N-terminal region is not ordered in electron density maps of different parvoviral capsid structures, plausibly due to low abundance of VP1 subunits and/or their asymmetric arrangement within the capsid (9). However, it is well known that the icosahedral two-fold constitutes the weakest interface in the AAV capsid (17, 18). Moreover, a recent structural study with AAV8 capsids at different pH values revealed a further decrease (~5%) in association energy and buried surface area at the two-fold interface under acidic conditions (27). Thus, it is likely that buried VP N-termini are externalized through openings at the two-fold interface as opposed to their extrusion through the five-fold pore (Figure 6), as postulated earlier (5). Such a mechanism is consistent with the observation that generation of inter-subunit dityrosine crosslinks, which would stitch together the two-fold interface, hinders externalization of VP N-termini resulting in decreased transduction efficiency of crosslinked AAV virions in cell culture.

Alternatively, it is possible that constraining the two-fold interface also restricts structural transitions required to open the five-fold pore. Previous studies with MVM have shown that the five symmetry-related copies of a conserved leucine residue, located at the base of each pentamer, appear to form a portal resembling an iris diaphragm at the base of each pore (7). Mutation of this conserved leucine appears to exert a destabilizing effect on MVM capsids resulting in premature exposure of VP1 N-termini. In contrast, similar mutagenesis studies carried out in AAV2 capsids report a decrease in pore flexibility, which prevents VP1u domain exposure (6, 12). Although the structures of AAV and MVM capsid five-fold pores are markedly different, it is interesting to note that mutation of residues positioned around the base or on the inner wall of the cylindrical pore exerts a deleterious effect on VP1u domain exposure in both parvoviruses (6, 28). Thus, constraining the AAV capsid two-fold depression could indeed alter the flexibility of the pentamer interface, which in turn is likely to block opening of the iris-like, five-fold pore (Figure 6B). Further high resolution structural studies are required to understand the exact mechanism of VP1u domain externalization in parvoviruses. Nevertheless, the current studies provide new insight into the role of interfacial capsid dynamics in exposure of hidden VP1 N-termini during parvoviral infection.

MATERIALS AND METHODS

Molecular modeling

The crystal structure of the AAV2 VP3 monomer (PDB ID: 1lp3) (17) was used as a template for modeling studies. Models of the AAV capsid (60 VP3 subunits) and trimers were obtained using the oligomer generator tool in the VIPERdb2 database (29) (http://viperdb.scripps.edu/). Surface rendered and cartoon models of capsid subunits were generated using the program PyMol (The PyMOL Molecular Graphics System, Schrödinger LLC, http://www.pymol.org/).

Cells and plasmids

Adherent human embryonic kidney (HEK293) and HeLa cells were grown at 37 °C in 5% CO_2 with Dulbecco's Modified Eagle Medium containing 10% fetal bovine serum and 1% penicillin/streptomycin/amphotericin B (MediaTech). Plasmids pXR2 (AAV2 helper containing *Rep* and *Cap* genes) and pXX6-80 (Adenovirus helper genes) were obtained from the UNC Vector Core. The pTR-CBA-Luc packaging construct containing chicken-beta actin (CBA) promoter-driven firefly luciferase transgene (Luc) has been described earlier (30).

Generation of AAV2 capsid mutants

The plasmid pXR2 was utilized as a template for site-directed mutagenesis to generate Y700F, Y704F, and Y730F mutations in the surface loop region of each VP subunit located near the two-fold depression. All mutagenesis reactions using different oligonucleotide primers (IDT) (Supplementary Table S1), were carried out as per manufacturer instructions outlined in the Quikchange XL® site-directed mutagenesis kit (Agilent Technologies). Individual clones were sequenced at the UNC Genome Analysis facility and capsid sequences analyzed using VectorNTI® software (Invitrogen).

Virus production and characterization

Recombinant AAV2 vectors packaging the CBA-Luc cassette were produced in HEK293 cells using the triple plasmid transfection method (31) At 60hrs post-transfection, cells were harvested and processed using cesium chloride gradient followed by sucrose gradient ultracentrifugation and dialysis. Viral titers were determined by quantitative PCR in a Roche Lightcycler® with primers specific for the Luc transgene region (Supplementary Table S1).

Chemical crosslinking of AAV capsids

Viral capsids (~1×10^{10} vector genomes) were crosslinked using 10mM Ni/GGH and 10mM magnesium monoperoxyphthalate (MMPP) (Sigma-Aldrich). Ni/GGH was prepared by combining equal parts nickel (II) acetate and Gly-Gly-His tripeptide. Capsids were reacted for 20hrs at room temperature. Reactions were then quenched using 150mM β-mercaptoethanol (Sigma-Aldrich) and dialyzed against 1× phosphate buffered saline (1× PBS). Control reactions without Ni/GGH and MMPP were also setup at room temperature and treated with β-mercaptoethanol after 20hrs. For electron microscopy, virus preps (unmodified or crosslinked) were loaded onto a 400 μm mesh carbon-coated copper grid followed by staining in 2% uranyl acetate. Images were captured using a Zeiss Leo 910 EM transmission electron microscope.

Western and dot blots

For western blots, crosslinked and control virus (1×10^{10} vector genomes) were separated on either NuPAGE 3–8% tris-acetate or 10% Bis/Tris gels (Invitrogen) in 1× tris-acetate or MOPS running buffer (150V, 1hr). Protein bands were transferred onto nitrocellulose using 1× transfer buffer supplemented with 30% methanol (30V, 1hr). For dot blots (far westerns), 2×10^{9} vector genomes were loaded directly onto a nitrocellulose membrane using a dot blot apparatus. Western blots were carried out with mouse monoclonal antibodies A1 (recognizing VP1 N-terminal domain), A69 (recognizing VP1/VP2 N-termini), B1 (recognizing VP1/VP2/VP3 C-terminal domain), and A20 (recognizing intact AAV2 capsids) (26) in hybridoma media (diluted 1:30) obtained from the UNC Vector Core and a goat anti-mouse secondary antibody conjugated to horseradish peroxidase (diluted 1: 5000). Western bands were visualized using SuperSignal West Femto Sensitivity Substrate (Thermo Scientific) and were captured using Amersham Hyperfilm ECL film (GE Healthcare). Western film was developed using a Konica Minolta SRX-101A developer.

In vitro transduction assays

HEK293 cells were seeded at 2×10^{5} cells per well in a 24-well plate format and transduced 18hrs later with different AAV2 vectors packaging the CBA-Luc cassette (MOI = 100). Transgene expression was determined by luminometric analysis with D-luciferin substrate (Promega) using a Victor® luminometer (Perkin Elmer) at 18hrs post-infection.

Confocal Microscopy

HeLa cells were seeded on poly-lysine coated coverslips placed in a 24-well plate at 10^5 cells per well and grown at 37 °C with 5% CO_2. After 18hrs, crosslinked or unmodified virus was added at a multiplicity of infection (MOI) of 50,000 vector genomes per cell. Cells were fixed with 2% paraformaldehyde, permeabilized with 0.2% Triton X-100, and blocked with immunofluorescence wash buffer (20 mM Tris pH 7.5, 137 mM NaCl, 3 mM KCl, 1.5 $MgCl_2$, 5mg mL^{-1} BSA, 0.05% Tween). Following cellular uptake, intact AAV particles were detected by immunostaining with mouse αCapsid (A20, American Research Products), while exposed VP1u domains were detected using the rabbit αVP1 (aa 2–16) described earlier (14). DyLight 488-conjugated goat anti-mouse and DyLight 594-conjugated goat anti-rabbit secondary antibodies (Pierce Scientific) were utilized for detection by immunofluorescence. Cells were then mounted with Prolong Gold anti-fade with DAPI® mounting media (Invitrogen) and imaged using a Zeiss LSM 710 confocal microscope. Images were captured with parameters including gain, laser power, and offset for each sample held constant. Analysis of confocal images was carried out after background correction using ImageJ® software. The mean fluorescence intensity ratio (αVP1u/A20) represents the fluorescent signal (DyLight 594) arising from exposed VP1u domains normalized to the fluorescent signal (DyLight 488) that corresponds to the total amount of internalized AAV2 particles. Histograms of mean fluorescence intensity ratios obtained from cells (total 30–50 count each) treated with either unmodified or crosslinked AAV2 capsids were then generated.

Supplementary Material

Refer to Web version on PubMed Central for supplementary material.

Acknowledgments

This work was funded by grants (awarded to A.A.) from NIH (R01HL089221, R01HL089221-S2). We would like to thank M. Agbandje-McKenna (University of Florida) for helpful comments as well as N. Pulicherla and S. Shen for helpful discussions. We would also like to thank V. Madden and R. Bagnell at the UNC microscopy services laboratory for technical guidance.

REFERENCES

1. Ros C, Gerber M, Kempf C. Conformational Changes in the VP1-Unique Region of Native Human Parvovirus B19 Lead to Exposure of Internal Sequences that Play a Role in Virus Neutralization and Infectivity. J. Virol. 2006; 80:12017–12024. [PubMed: 17020940]
2. Nelson CD, Minkkinen E, Bergkvist M, Hoelzer K, Fisher M, Bothner B, Parrish CR. Detecting Small Changes and Additional Peptides in the Canine Parvovirus Capsid Structure. J. Virol. 2008; 82:10397–10407. [PubMed: 18701590]
3. Lindert S, Silvestry M, Mullen TM, Nemerow GR, Stewart PL. Cryo-Electron Microscopy Structure of an Adenovirus-Integrin Complex Indicates Conformational Changes in both Penton Base and Integrin. J. Virol. 2009; 83:11491–11501. [PubMed: 19726496]
4. Trask SD, Kim IS, Harrison SC, Dormitzer PR. A Rotavirus Spike Protein Conformational Intermediate Binds Lipid Bilayers. J. Virol. 2010; 84:1764–1770. [PubMed: 20007281]
5. Kronenberg S, Bottcher B, von der Lieth CW, Bleker S, Kleinschmidt JA. A Conformational Change in the Adeno-Associated Virus Type 2 Capsid Leads to the Exposure of Hidden VP1 N Termini. J. Virol. 2005; 79:5296–5303. [PubMed: 15827144]
6. Bleker S, Sonntag F, Kleinschmidt JA. Mutational Analysis of Narrow Pores at the Fivefold Symmetry Axes of Adeno-Associated Virus Type 2 Capsids Reveals a Dual Role in Genome Packaging and Activation of Phospholipase A2 Activity. J. Virol. 2005; 79:2528–2540. [PubMed: 15681453]

7. Farr GA, Cotmore SF, Tattersall P. VP2 Cleavage and the Leucine Ring at the Base of the Fivefold Cylinder Control pH-Dependent Externalization of both the VP1 N Terminus and the Genome of Minute Virus of Mice. J. Virol. 2006; 80:161–171. [PubMed: 16352540]
8. Bowles, DE.; Rabinowitz, JE.; Samulski, RJ. The Genus *Dependovirus*,. In: Kerr, JR.; Cotmore, SF.; Bloom, ME.; Linden, RM.; Parrish, CR., editors. Parvoviruses. 2006.
9. Chapman, MS.; Agbandje-McKenna, M. Atomic Structure of Viral Particles. In: Kerr, JR.; Cotmore, SF.; Bloom, ME.; Linden, RM.; Parrish, CR., editors. Parvoviruses. Edward Arnold Ltd; New York: 2006. p. 107-123.
10. Rose JA, Maizel JV Jr, Inman JK, Shatkin AJ. Structural Proteins of Adenovirus-Associated Viruses. J. Virol. 1971; 8:766–770. [PubMed: 5132697]
11. Buller RM, Rose JA. Characterization of Adenovirus-Associated Virus-Induced Polypeptides in KB Cells. J. Virol. 1978; 25:331–338. [PubMed: 621779]
12. Grieger JC, Johnson JS, Gurda-Whitaker B, Agbandje-McKenna M, Samulski RJ. Surface-Exposed Adeno-Associated Virus Vp1-NLS Capsid Fusion Protein Rescues Infectivity of Noninfectious Wild-Type Vp2/Vp3 and Vp3-Only Capsids but Not that of Fivefold Pore Mutant Virions. J. Virol. 2007; 81:7833–7843. [PubMed: 17507473]
13. Sonntag F, Bleker S, Leuchs B, Fischer R, Kleinschmidt JA. Adeno-Associated Virus Type 2 Capsids with Externalized VP1/VP2 Trafficking Domains are Generated Prior to Passage through the Cytoplasm and are Maintained Until Uncoating Occurs in the Nucleus. J. Virol. 2006; 80:11040–11054. [PubMed: 16956943]
14. Johnson JS, Li C, DiPrimio N, Weinberg MS, McCown TJ, Samulski RJ. Mutagenesis of Adeno-Associated Virus Type 2 Capsid Protein VP1 Uncovers New Roles for Basic Amino Acids in Trafficking and Cell-Specific Transduction. J. Virol. 2010; 84:8888–8902. [PubMed: 20573820]
15. Girod A, Wobus CE, Zadori Z, Ried M, Leike K, Tijssen P, Kleinschmidt JA, Hallek M. The VP1 Capsid Protein of Adeno-Associated Virus Type 2 is Carrying a Phospholipase A2 Domain Required for Virus Infectivity. J. Gen. Virol. 2002; 83:973–978. [PubMed: 11961250]
16. Stahnke S, Lux K, Uhrig S, Kreppel F, Hosel M, Coutelle O, Ogris M, Hallek M, Buning H. Intrinsic Phospholipase A2 Activity of Adeno-Associated Virus is Involved in Endosomal Escape of Incoming Particles. Virology. 2011; 409:77–83. [PubMed: 20974479]
17. Xie Q, Bu W, Bhatia S, Hare J, Somasundaram T, Azzi A, Chapman MS. The Atomic Structure of Adeno-Associated Virus (AAV-2), a Vector for Human Gene Therapy. Proc. Natl. Acad. Sci. U. S. A. 2002; 99:10405–10410. [PubMed: 12136130]
18. Govindasamy L, Padron E, McKenna R, Muzyczka N, Kaludov N, Chiorini JA, Agbandje-McKenna M. Structurally Mapping the Diverse Phenotype of Adeno-Associated Virus Serotype 4. J. Virol. 2006; 80:11556–11570. [PubMed: 16971437]
19. Nam HJ, Lane MD, Padron E, Gurda B, McKenna R, Kohlbrenner E, Aslanidi G, Byrne B, Muzyczka N, Zolotukhin S, Agbandje-McKenna M. Structure of Adeno-Associated Virus Serotype 8, a Gene Therapy Vector. J. Virol. 2007; 81:12260–12271. [PubMed: 17728238]
20. Ng R, Govindasamy L, Gurda BL, McKenna R, Kozyreva OG, Samulski RJ, Parent KN, Baker TS, Agbandje-McKenna M. Structural Characterization of the Dual Glycan Binding Adeno-Associated Virus Serotype 6. J. Virol. 2010; 84:12945–12957. [PubMed: 20861247]
21. Lerch TF, Xie Q, Chapman MS. The Structure of Adeno-Associated Virus Serotype 3B (AAV-3B): Insights into Receptor Binding and Immune Evasion. Virology. 2010; 403:26–36. [PubMed: 20444480]
22. Meunier S, Strable E, Finn MG. Crosslinking of and Coupling to Viral Capsid Proteins by Tyrosine Oxidation. Chem. Biol. 2004; 11:319–326. [PubMed: 15123261]
23. Zhong L, Li B, Mah CS, Govindasamy L, Agbandje-McKenna M, Cooper M, Herzog RW, Zolotukhin I, Warrington KH Jr, Weigel-Van Aken KA, Hobbs JA, Zolotukhin S, Muzyczka N, Srivastava A. Next Generation of Adeno-Associated Virus 2 Vectors: Point Mutations in Tyrosines Lead to High-Efficiency Transduction at Lower Doses. Proc. Natl. Acad. Sci. U. S. A. 2008; 105:7827–7832. [PubMed: 18511559]
24. Gill G, Richter-Rusli AA, Ghosh M, Burrows CJ, Rokita SE. Nickel-Dependent Oxidative Cross-Linking of a Protein. Chem. Res. Toxicol. 1997; 10:302–309. [PubMed: 9084910]

25. Brown KC, Yang SH, Kodadek T. Highly Specific Oxidative Cross-Linking of Proteins Mediated by a Nickel-Peptide Complex. Biochemistry. 1995; 34:4733–4739. [PubMed: 7718579]

26. Wobus CE, Hugle-Dorr B, Girod A, Petersen G, Hallek M, Kleinschmidt JA. Monoclonal Antibodies Against the Adeno-Associated Virus Type 2 (AAV-2) Capsid: Epitope Mapping and Identification of Capsid Domains Involved in AAV-2-Cell Interaction and Neutralization of AAV-2 Infection. J. Virol. 2000; 74:9281–9293. [PubMed: 10982375]

27. Nam HJ, Gurda BL, McKenna R, Potter M, Byrne B, Salganik M, Muzyczka N, Agbandje-McKenna M. Structural Studies of AAV8 Capsid Transitions Associated with Endosomal Trafficking. J. Virol. 2011; 85:11791–11799. [PubMed: 21900159]

28. Reguera J, Carreira A, Riolobos L, Almendral JM, Mateu MG. Role of Interfacial Amino Acid Residues in Assembly, Stability, and Conformation of a Spherical Virus Capsid. Proc. Natl. Acad. Sci. U. S. A. 2004; 101:2724–2729. [PubMed: 14981262]

29. Carrillo-Tripp M, Shepherd CM, Borelli IA, Venkataraman S, Lander G, Natarajan P, Johnson JE, Brooks CL 3rd, Reddy VS. VIPERdb2: An Enhanced and Web API Enabled Relational Database for Structural Virology. Nucleic Acids Res. 2009; 37:D436–42. [PubMed: 18981051]

30. Pulicherla N, Shen S, Yadav S, Debbink K, Govindasamy L, Agbandje-McKenna M, Asokan A. Engineering Liver-Detargeted AAV9 Vectors for Cardiac and Musculoskeletal Gene Transfer. Mol. Ther. 2011; 19:1070–1078. [PubMed: 21364538]

31. Grieger JC, Choi VW, Samulski RJ. Production and Characterization of Adeno-Associated Viral Vectors. Nat. Protoc. 2006; 1:1412–1428. [PubMed: 17406430]

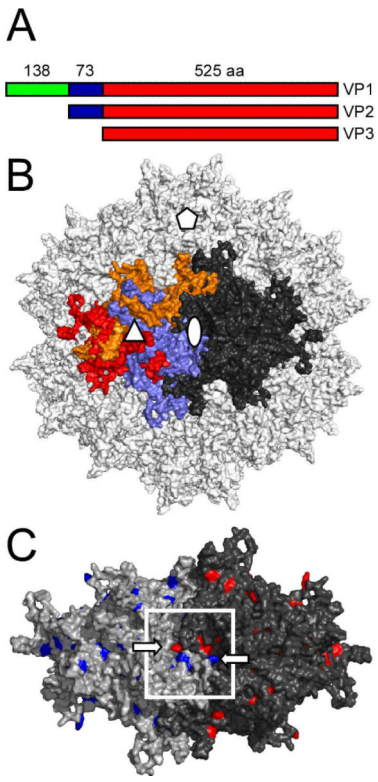

FIGURE 1.

3D mapping of surface-exposed tyrosines at the two-fold interface on the AAV2 capsid. (A) Schematic alignment of the three AAV structural proteins VP1, VP2 and VP3 which make up the capsid. (B) 3D surface model of the AAV2 capsid (PDB ID: 1LP3) containing 60 monomer subunits colored light grey with the icosahedral two-fold (oval), three-fold (triangle) and five-fold symmetry (pentagon) highlighted in white. Monomer subunits forming a trimer are colored pale green, wheat and salmon with the neighboring trimer colored in dark grey. (C) 3D surface model of a dimer of trimers shown in light and dark grey with corresponding surface-exposed tyrosine residues highlighted in blue and red, respectively. The two-fold depression is highlighted within the white boxed region showing a cluster of surface-exposed tyrosine residues. The Tyr704 residue, which extends from one overlapping capsid protein subunit into the neighboring subunit at the two-fold interface, is highlighted with white arrows. All images were generated and rendered in PyMol®.

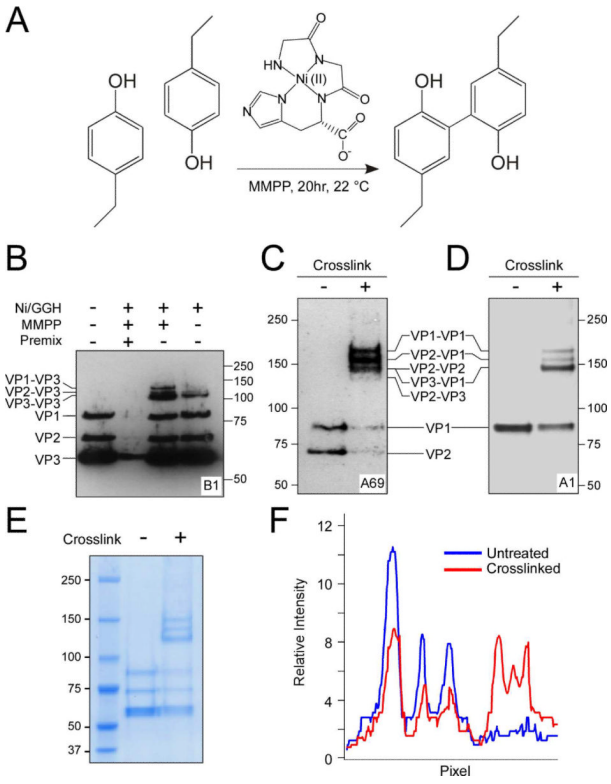

FIGURE 2.

Site-selective chemical crosslinking of AAV2 capsid subunit dimers. (A) Schematic of chemical reaction involving treatment of tyrosine side chains with the Ni(II)/GGH complex to form a dityrosine covalent linkage. (B) Western blot of denatured AAV2 capsid proteins in unmodified or crosslinked form with the B1 monoclonal antibody (MAb), which detects the C-terminal domain of all AAV2 VP subunits. Stepwise addition of individual chemical reagents yielded optimal reaction conditions for crosslinked VP dimer formation. Different permutations and combinations of VP subunit dimers are labeled based on predicted molecular weight. Additional dimers are visualized using (C) the A69 MAb, which recognizes both VP1 and VP2 subunits and (D) the A1 MAb, which recognizes only VP1 subunits. Absolute protein levels of native and crosslinked VP subunits was determined by SDS-PAGE stained with colloidal blue (E) followed by cross-sectional analysis of the different lanes with Igor Pro data analysis software (F).

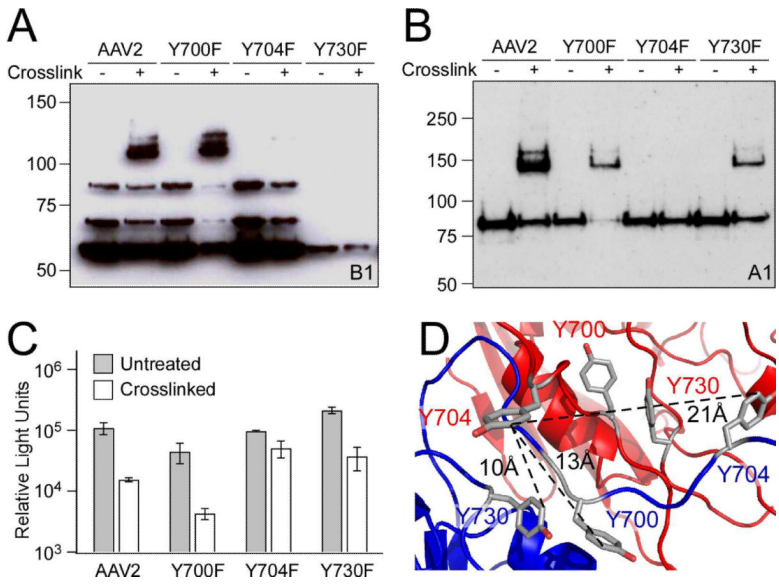

FIGURE 3.

Tyr-to-Phe mutants reveal molecular mechanisms underlying the formation of crosslinked VP dimers. Western blots of denatured, wild type (wt) and mutant AAV2 capsid proteins in unmodified (−) or crosslinked form (+) with B1 (A) and A1 (B) MAbs. (C) Transduction efficiency (luciferase expression) of unmodified (grey bars) and crosslinked (white bars) wtAAV2 and Tyr-to-Phe mutants in HEK293 cells (Multiplicity of infection, MOI = 100vg/cell). Error bars represent standard deviation (n=3). (D) Cartoon of the AAV2 capsid two-fold interface with neighboring VP subunits colored red and blue. Different tyrosine residues in each VP subunit are highlighted in the corresponding color. The Y704 residue in one VP subunit monomer and extends into the neighboring subunit and lies adjacent to the Y730 residue and to a lesser extent the Y700 residue. Distances between the Y704 3′ carbon from the red monomer and the 3′ carbons for Y730, Y700, and Y704 from the blue monomer are shown in black. This unique structural arrangement of tyrosines at the two-fold interface is the driving-force behind dityrosine adduct formation, which yields crosslinked VP subunit dimers.

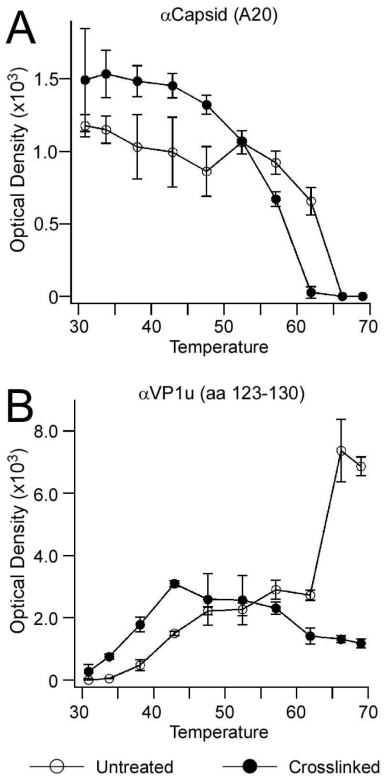

FIGURE 4.

Temperature-dependent exposure of the VP1 N-terminal domain in unmodified (◯) and crosslinked (●) AAV2 capsids. Unmodified and crosslinked capsids were heated to different temperatures for 30min prior to dot blot analysis. The intact capsid was detected by the conformation-specific MAb A20 (A) and MAb A1 (B) was used to detect the exposed VP1 N-terminal domain. Optical densities were measured using a Kodak® gel documentation system equipped with an optical filter. Error bars represent standard deviation (n=3).

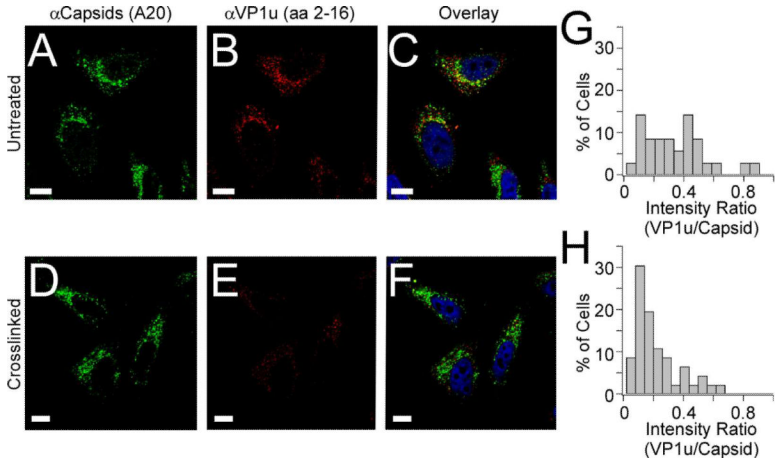

FIGURE 5.

Immunofluorescent confocal micrographs of HeLa cells treated with unmodified (top panel) or crosslinked (bottom panel) AAV2 capsids (MOI 50,000vg/cell). Images were obtained at 24hrs post-infection with the MAb A20 to detect intact AAV2 capsids (DyLight-488® green) (A & D) and the MAb αVP1 to detect exposed VP1 N-termini (DyLight-594® red) (B & E). Image overlay demonstrating co-localized staining of intact capsids with exposed VP1 N-termini (yellow) is also shown (C & G). Nuclei were stained blue using DAPI. All images were obtained using a Zeiss LSM 710 confocal fluorescence microscope (Scale = 10μm). Mean fluorescence ratios (αVP1/A20) of individual cells were calculated after background subtraction. (G) Cells infected with unmodified AAV2 capsids display peak intensity ratios at 0.1 and 0.4, with nearly 15% of the cells in each subset, suggesting that a significant population of AAV2 virions contains exposed VP1 N-termini. (n=32). (H) Cells infected with crosslinked AAV2 capsids display a peak intensity ratio of 0.1 with 30% of the cells located within this subset, supporting a significant increase in the population of AAV2 capsids defective in externalization of VP1 N-termini (n=46).

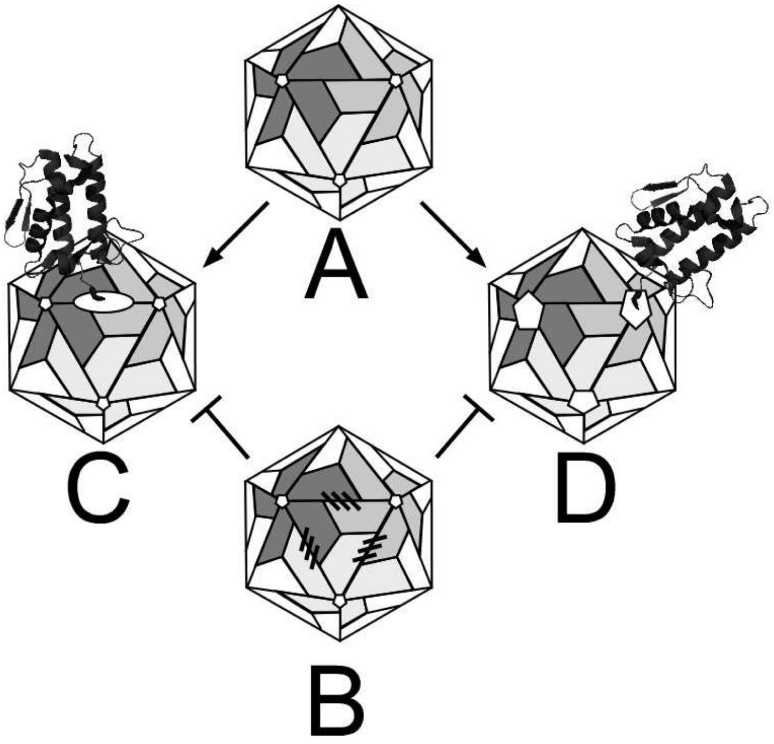

FIGURE 6.

Two models of VP1u exposure during infection. The VP1u domain represented as a black ribbon drawing was adapted from the structure of porcine pancreatic phospholipase [PDB ID: 3O4M] and is initially buried within the capsid (A). Tyrosine-crosslinked capsids (B) are unable to expose their VP1u domain either by preventing opening of the two-fold symmetry axis (C) or iris-like opening of the five-fold pore (D). VP monomers are represented as trapezoids in white, light grey or dark grey; the open two-fold axis is represented as a white oval and five-fold pores are represented as white pentagons.